ЖЭТФ, 2002, том 121, вып. 1, стр. 210–224

LATTICE RELAXATION AND CHARGE-TRANSFER OPTICAL TRANSITIONS DUE TO SELF-TRAPPED HOLES IN NONSTOICHIOMETRIC $LaMnO_3$ CRYSTAL

N. N. Kovaleva [ab*], *J. L. Gavartin* [b], *A. L. Shluger* [b], *A. V. Boris* [ac], *A. M. Stoneham* [b]

[a] *Institute of Solid State Physics, Russian Academy of Sciences*
142432, Chernogolovka, Moscow Region, Russia

[b] *University College London*
London WC1E 6BT, United Kingdom

[c] *Max-Planck-Institut für Festkörperforschung*
70569, Stuttgart, Germany

Submitted 12 April 2001

We explore the role of electronic and ionic polarization energies in the physics of the «colossal» magnetoresistive (CMR) materials. We use the Mott–Littleton approach to evaluate polarization energies in the $LaMnO_3$ lattice associated with holes localized on both the Mn^{3+} cation and O^{2-} anion. The full (electronic and ionic) lattice relaxation energy for a hole localized at the O site is estimated as 2.4 eV, which is appreciably greater than that of 0.8 eV for a hole localized at the Mn site, indicating a strong electron–phonon interaction in the former case. The ionic relaxation around the localized holes differs for the anion and cation holes. The relaxation associated with Mn^{4+} is approximately isotropic, whereas ionic displacements around O^- holes show axial symmetry with the axis directed towards the apical oxygens. Using the Born–Haber cycle, we examine thermal and optical energies of the hole formation associated with the electron ionization from Mn^{3+}, O^{2-}, and La^{3+} ions in the $LaMnO_3$ lattice. For these calculations, we derive a phenomenological value for the second electron affinity of oxygen in the $LaMnO_3$ lattice by matching the optical energies of the La^{4+} and O^- hole formation with maxima of binding energies in the experimental photoemission spectra. The calculated thermal energies predict that the electronic hole is marginally more stable in the Mn^{4+} state in the $LaMnO_3$ host lattice, but the energy of a hole in the O^- state is only higher by a small amount, 0.75 eV, suggesting that both possibilities should be treated seriously. We examine the energies of a number of fundamental optical transitions, as well as those involving self-trapped holes of Mn^{4+} and O^- in the $LaMnO_3$ lattice. The reasonable agreement of our predicted energies, linewidths, and oscillator strengths with experimental data leads us to plausible assignments of the optical bands observed. We deduce that the optical band near 5 eV is associated with the $O(2p)$–$Mn(3d)$ transition of a charge-transfer character, whereas the band near 2.3 eV is rather associated with the presence of Mn^{4+} and/or O^- self-trapped holes in the nonstoichiometric $LaMnO_3$ compound.

PACS: 75.30.Vn, 71.55.Ht, 78.40.Ha

1. INTRODUCTION

The striking behavior of the «colossal» magnetoresistive (CMR) oxides of $R_{1-x}A_xMnO_3$ (where R stands for trivalent rare-earth ions and A for divalent alkaline-earth ions, and $0.2 \leq x \leq 0.5$) arises from the interplay of several distinct energy terms: magnetic interactions, electronic band structure energies, crystal field splittings, vibrational energies, and the electron–lattice coupling, including small polaron ideas and the Jahn–Teller (JT) effect. Understanding this behavior has been helped very greatly by the use of models to map the various regimes of behavior [1]. The experimental evidence [2] suggests that manganites are doped charge-transfer insulators having $O(2p)$ holes rather than Mn^{3+} $(3d)$ electrons as the current carriers. How-

*E-mail: nkovalev@issp.ac.ru

ever, whether holes reside at O and/or Mn sites is still the subject of controversy. Some of the models of polarization and vibration in CMR systems make major approximations, such as a single vibrational frequency (Einstein model) or rigid, unpolarizable ions. These simplifications are known to give seriously inadequate results, both quantitatively and qualitatively. For example, for the charge transfer transitions of the zinc vacancy center V^- in ZnSe, optical spectroscopy [3] allows one to obtain the key relaxation and tunnelling energies. But in the simple one-frequency rigid-ion model, these values are inconsistent with the observed charge localization on a single Se neighbor to the vacancy [4]. However, the consistency and good agreement with experiment are restored in the general model at the harmonic and dipole approximation level, namely the shell model. Important properties of the shell model [5, 6] consist, first, in properly separating the ionic and electronic polarizations, such that phonons are well predicted and polarization at the atomic scale is well reproduced, and second, in recognizing that the local environment affects the polarizability of ions through short-range repulsive forces. As a result, the shell model provides an adequate framework for understanding energies dominated by polarization and distortion. Such energies include those describing small polarons [3–5] and optical charge transfer transitions (as considered for MgO [7] and V^- centers in ZnSe [4]). The shell model has also been extensively used in studies of defect energetics and nonstoichiometry in oxides [8]. Its considerable quantitative success arises largely because it provides such an accurate description of the large polarization energies.

It is helpful to recognize the orders of magnitude of the several energy terms for CMR oxides. Obviously, a small energy does not mean that the particular energy is unimportant, but a small value often means that very simple ideas for those terms are sufficient in examining phenomena dominated by large energies. Typical magnitudes are as follows.

CMR instability energy of an electron in an external field of 10 T ..... 0.001 eV ($\sim \mu_B g H$).

Magnetic exchange (from kT_N, with T_N being the Neel temperature) ..... 0.01 eV.

Energy of the noncubic structural deformation of the $LaMnO_3$ cell ..... $\leq$ 0.4 eV.

Jahn–Teller energy (from the largest known JT energies) ..... $\leq$ 0.4 eV.

Crystal-field splitting energies (from data on many systems) ..... 1 eV typical.

Polarization energies (net charge $\pm e$) ... 5 to 10 eV.

Free-ion ionization potentials ..... tens of eV.

Madelung energies (fully ionic models).. tens of eV.

In this paper, we mainly consider the polarization energies, for which the large energy terms are dominant. We only discuss the JT and crystal field energies in simple terms, although we remark that one-frequency models of the JT effect also lead to inconsistencies.

We apply the shell model calculations to look specifically at energies associated with the localized holes of Mn^{4+} and O^- in a nonstoichiometric or slightly doped «parent» $LaMnO_3$ compound. Using this model, we address some of the issues in physics of CMR systems for which the polarization energies are crucial. First, we calculate the electronic and ionic polarization energies due to holes localized on Mn^{3+} and O^{2-} ions in order to estimate the key polaron energies and examine the controversial question whether holes reside at Mn or O sites in the $LaMnO_3$ lattice. Second, we estimate the energies of the main charge transfer transitions including Mn^{4+} and O^- species, which determine specific transport properties of doped CMR materials. We analyze their contribution to the optical conductivity in the nonstoichiometric $LaMnO_3$ crystal and make the assignment of bands in the optical conductivity spectrum more clear-cut.

2. DESCRIPTION OF THE $LaMnO_3$ SYSTEM AND THE SHELL MODEL APPROXIMATION

Many of the CMR materials are hole-doped systems of perovskite manganites of the form $La_{1-x}A_xMnO_3$. Their properties are intimately related to those of the «parent» compound ($x = 0$). Below $T_N \approx 140$ K, $LaMnO_3$ is an A-type antiferromagnet in which the MnO_2 ferromagnetic layers are stacked along the c axis with alternating spin directions. The structure of the perovskite manganites can be clearly understood starting from the simple cubic perovskite structure ($Pm3m$). The idealized cubic structure of $LaMnO_3$ featuring a chain of the corner-sharing MnO_6 octahedra is presented in Fig. 1. The Mn^{3+} ion with the $3d^4$ electronic configuration is known to exhibit a large JT effect in other systems [9]. Therefore, it is natural to assume that the JT instability of the Mn^{3+} ion can contribute to an orthorhombic distortion of the perovskite structure of the $Pnma$ symmetry in the $LaMnO_3$ crystal. The orthorhombic structure can be obtained from the cubic perovskite structure by two consequent and co-

Fig. 1. The idealized cubic perovskite structure ($Pm3m$) of the $LaMnO_3$ crystal. The orthorhombic $Pnma$ structure can be obtained by two consequent rotations of the MnO_6 octahedra around the [010] and [101] directions

ordinated rotations of the MnO_6 octahedra around the [010] and [101] directions, as shown in Fig. 1. Another possible contribution to the observed distortion from the cubic symmetry in $LaMnO_3$ could be attributed to an atomic size mismatch: the sum of the Mn–O layer ionic radii, $r_{Mn} + r_O$, does not match that of the La–O layer, $(r_{La} + r_O)/\sqrt{2}$, in the right way for a stable cubic structure. The size mismatch effect is known to be a common reason for distortions in different perovskite oxides. Our shell model calculations performed for the $LaMnO_3$ $Pnma$ structure indicate that the orthorhombic distortions experimentally observed at low temperatures could not be simply caused by the lattice mismatch effect (which, in principle, must be properly described in the framework of the shell model approximation), but are caused by the both effects, with a comparative contribution of the JT effect. Some special efforts should be undertaken to empirically account for the JT effect in the framework of the shell model. We perform the shell model calculations for the cubic perovskite structure (Fig. 1). This approximation seems to be mostly relevant to the nonmagnetic quasi-cubic perovskite structure of the $LaMnO_3$ crystal experimentally observed at high temperatures $T \geq 400$ K $> T_N \approx 140$ K. We suggest that our modeling of the cubic perovskite structure provides a reasonable model because we are mainly interested in estimating the key polarization energies associated with polaron-type charge carriers in the high-temperature insulating quasi-cubic phase of the CMR lattices.

We model the $LaMnO_3$ system using methods based on the shell model and the Mott–Littleton approach that have been successfully applied to studying the properties of a wide range of oxides (including transition metal oxides), halides, and other systems [10, 11]. The calculations are performed using the GULP code [12]. In the shell model [5], the lattice is considered as an assembly of polarizable ions, represented by massive point cores and massless shells coupled by isotropic harmonic forces. The interaction potential includes contributions of the Coulomb, polarization, and short-range interactions. We adopt a fully ionic model (with the formal charges of ions in the $LaMnO_3$ lattice, La^{3+}, Mn^{3+}, and O^{2-}). This is less restrictive than one might think because a parallel covalent description is possible [13]. The sum of the core and shell charges is equal to the formal charge of the ion in the lattice. The core and shell charges and the spring constant of each ion are parameters of the model. The electronic polarization of the ions is represented by the displacement of their shells relative to the cores in the dipole approximation. The lattice distortion is simulated by the core displacements from their lattice site positions.

In our model, cations are treated as unpolarizable and the short-range interactions between relatively small cations (core–core interactions) are ignored. The short-range potentials used for the shell–shell (oxygen–oxygen) and core–shell (metal–oxygen) interactions are of the Buckingham form,

$$V_{ij} = A_{ij} \exp\left(-\frac{r}{\rho_{ij}}\right) - \frac{C_{ij}}{r^6}. \qquad (1)$$

The parameters of both repulsive and attractive components of the Buckingham potential for the shell–shell (O^{2-}–O^{2-}) interactions used in this work are obtained in Ref. [14] and presented in Table 1(a). The Buckingham parameters for the core–shell Mn^{3+}–O^{2-} and La^{3+}–O^{2-} interactions were fitted in this work using the experimental data including the lattice parameter, the static and high-frequency dielectric constants, and the frequencies of the transverse optical (TO) phonons in the $LaMnO_3$ crystal [15]. The dielectric constants are especially important if one wishes to predict polarization energies accurately. We have not found an experimental value of the static dielectric constant of $LaMnO_3$ in the literature. We are grateful to T. Arima and Y. Tokura [16] for sending us the experi-

Table 1. Potential parameters for short-range interactions in $LaMnO_3$ ($Pm3m$): (a) elaborated in the present work; (b) from Islam et al. [17]; (c) from Grimes [20] for Mn^{3+} and Mn^{4+} different valence states; $r_{cutoff} = 20$ Å

		A, eV	ρ, Å	C, eV·Å^{-6}	Y, $\lvert e\rvert$	k, eV·Å^{-2}
(a)	La^{3+}–O^{2-}	1516.3	0.3639	0.00		
	Mn^{3+}–O^{2-}	1235.9	0.31525	0.00		
	O^{2-}–O^{2-}	22764.3	0.1490	20.37	−2.48	16.8
(b)	La^{3+}–O^{2-}	1516.3	0.3525	0.00		
	Mn^{3+}–O^{2-}	1235.9	0.3281	0.00		
	O^{2-}–O^{2-}	22764.3	0.1490	43.00		
(c)	La^{3+}–O^{2-}	2088.79	0.3460	23.25		
	Mn^{3+}–O^{2-}	922.83	0.3389	0.00		
	Mn^{4+}–O^{2-}	1386.14	0.3140	0.00		
	O^{2-}–O^{2-}	9547.96	0.2192	32.00	−2.04	6.3

mental data on the reflectivity spectra of $LaMnO_3$ measured at room temperature and reported in Ref. [15]. In the present work, the experimental value of the static dielectric constant $\epsilon_0 \approx 18 \pm 2$ was derived from these data by the Kramers–Kronig analysis and was further used in the fitting procedure. The parameters fitted for $LaMnO_3$ ($Pm3m$) in Ref. [17] (see Table 1(b)) were used as the starting values for the core–shell La^{3+}–O^{2-} and Mn^{3+}–O^{2-} short-range interaction potentials. The oxygen shell charge was taken as $-2.48|e|$ and the shell–core spring constant k was chosen to give the correct value of the static dielectric constant ϵ_0.

The final values of our shell model parameters are presented in Table 1(a). The calculated and experimental properties of $LaMnO_3$ ($Pm3m$) are summarized in Table 2. One can see that both sets of parameters (Table 1(a, b)) give close values for the lattice parameter and cohesive energy, however at the same time, our parameters give results that are close to the static and high-frequency dielectric constants. The value of the static dielectric constant calculated with the parameters given in Ref. [17] is much higher than that derived from the experimental reflectivity spectra. Our model also agrees well with the experimental values of the transverse optical phonon energies [15]. The phonon bands obtained in our calculations correlate well with those observed with higher oscillator strengths. In particular, the predicted phonon energies agree well for the La-external mode (ω_{TO_1}), Mn–O–Mn bending mode (ω_{TO_2}) and Mn–O stretching mode (ω_{TO_3}) for the quasi-cubic perovskite structure of the strongly doped perovskite manganite system $La_{0.67}Ca_{0.33}MnO_3$ [18, 19].

We have also tested another set of short-range pair potentials that are different for the Mn ion in different valence states Mn^{2+}, Mn^{3+}, and Mn^{4+}. The potentials were obtained by fitting the equilibrium structures of several oxide compounds, such as MnO, $LaMnO_3$, and Ca_2MnO_4 [20]. We tested pair potentials for Mn^{4+} and Mn^{3+} from this set, presented in Table 1(c). These parameters also give good results (see the set of values (c) in Table 2) for the lattice parameter and dielectric constants, but are less successful in predicting the optical phonon frequencies. As we show below, both these and our parameters give similar values for the calculated properties of polarons in these crystals, thereby validating the correctness of the shell model approach.

We then apply the shell model parameters to estimate key defect energies using the well-known Mott–Littleton method (see Ref. [11] for a more detailed description). It is based on the concept that the total energy of the crystal lattice containing a defect is minimized by relaxation of the ions surrounding the defect, and this relaxation fairly rapidly decreases at distances away from the defect. In these calculations, the crystal is divided into three regions: an inner spherical region I, containing the defect and its immediate surroundings, an intermediate finite region II, which is created to properly link region I, and an outer infinite region III, which responds as a dielectric continuum. Finite regions I and II are embedded in infinite region III. The typical radii of regions I and II used in our calculations were 10 and 25 Å, respectively. We considered an electronic hole located in the center of region I, which is

Table 2. Crystal properties of $LaMnO_3$ ($Pm3m$) calculated using the shell model potentials (Table 1) and compared with experimental data

	Lattice const. a_0, Å	Cohesive energy E_{lat}, eV	ϵ_0	ϵ_∞	ω_{TO_1}, cm^{-1}	ω_{TO_2}, cm^{-1}	ω_{TO_3}, cm^{-1}
Exp.	3.889		18 ± 2 [15]	4.9 [15]	172 [15]	360 [15]	560 [15]
Calc. (a)	3.889	−140.52	15.6	4.9	172	308	513
Calc. (b)	3.904	−139.12	56.17	–	–	–	–
Calc. (c)	3.906	−139.58	14.1	4.6	156	252	368

the most perturbed. The displacements of cores and shells in this region are calculated explicitly. In intermediate region II, the ions are also treated within the shell model, but their displacements and polarizations are derived from the dielectric continuum approximation. The system total energy is minimized (the preset accuracy was 0.01 eV) with respect to the positions of all cores and shells in regions I and II in the potential produced by polarized region III.

The Mott–Littletone method is especially valuable to estimate key polaron energies because the long-range polarization fields are treated properly; many other methods (such as cluster methods or periodic cell methods) treat these significant terms badly.

3. ELECTRONIC HOLES IN $LaMnO_3$

3.1. Relaxation energies of the localized holes in $LaMnO_3$

We study possible hole localization (self-trapping) on Mn^{3+} and O^{2-} ions in a slightly hole-doped or nonstoichiometric $LaMnO_3$ crystal. Theoretical predictions of the electron charge carrier self-trapping in the ideal lattice are based on calculations of the so-called self-trapping energy [10], which is the difference between the localization and relaxation energies. The first of these terms is basically an increase in the hole (electron) kinetic energy due to its localization on a finite number of lattice sites from a completely delocalized state. The second is the energy gain due to the lattice polarization by the localized charge. They represent a very delicate balance of large terms that in many cases differ by 0.1 eV only. The calculation of the localization energy, especially in complex crystals, is the most difficult part of the study of the electron charge carrier self-trapping [10] and requires accurate electronic structure calculations beyond the scope of this work. Our aim is rather to compare the relaxation energies for the hole localization in two different sublattices of the same crystal. These energies are indicative of the strength of the electron–phonon interaction, and their difference can suggest whether there are major differences in hole trapping in one of the sublattices.

The hole formation process can be generally seen as the ionization of the in-crystal ion with an electron being taken out of the crystal and put on the vacuum level. The energy required in this process (the hole formation energy E_h^α for α = Mn, O, La) is the work done against the in-crystal ionic core potential, I^α, and the crystalline electrostatic potential, U_M^α, less than the energy gain due to the lattice polarization effects, R^α:

$$E_h^\alpha = I^\alpha + U_M^\alpha + R^\alpha. \tag{2}$$

To assess the extent of the lattice perturbation by the hole localization and calculate the hole relaxation energy, it is useful to distinguish the «electronic» and «ionic» terms in the polarization energy. The first term, which we call R_{opt}^α, is due to the «electronic» polarization of ions by the momentarily localized hole, which in our method is represented by the displacements of shells with respect to the cores that are fixed at their perfect crystal positions. This term takes the lattice response on, e.g., the Franck–Condon photoionization into account. The lattice distortion term due to displacements of cores and related adjustment of shells after the complete lattice relaxation, denoted as ΔR_{th}^α, is the difference between the full polarization energy R^α and R_{opt}^α,

$$\Delta R_{th}^\alpha = R^\alpha - R_{opt}^\alpha. \tag{3}$$

It represents the hole relaxation energy. If this energy exceeds the localization energy, i.e., the kinetic energy rise due to the complete hole localization on this site,

one can then talk about the hole being self-trapped on this site. Given this assumption, Eq. (2) takes the form

$$E_h^\alpha = I^\alpha + U_M^\alpha + R_{opt}^\alpha + \Delta R_{th}^\alpha. \qquad (4)$$

The shell model Mott–Littleton calculations give the cumulative energy of the second and third terms, S_{opt}^α, or of the last three terms, S_{th}^α, in Eq. (4) depending on whether both shells and cores or shells only were allowed to relax. It is sensible, however, to evaluate these terms separately. This can be rigorously done by independently calculating the on-site electrostatic potential U_M^α within the periodic model and using the definition introduced by Eq. (3). The values of S_{opt}^α and S_{th}^α and the calculated terms U_M^α, R_{opt}^α, and ΔR_{th}^α are summarized in Table 3.

It follows from the calculations that there is a large difference in the lattice relaxation energies for the O^- and Mn^{4+} holes. The lattice relaxation energy $-\Delta R_{th}^\alpha$ caused by the hole localization at the O site (2.38 eV) appears to be significantly larger than that for the hole localized at the Mn site (0.83 eV), as shown in Table 3(a). This indicates a strong electron–phonon interaction in the case of the hole localized at the O site and could suggest that the hole trapping is more preferential in the oxygen sublattice. However, the width of the Mn($3d$) subband in the density of states, which determines the hole localization energy, is much narrower than that of the O($2p$) related subband [21]. Without a much fuller electronic structure calculation of the localization energy, it is therefore impossible to draw any final conclusion as to in which sublattice the holes could be localized.

One experimental test could involve the analysis of local vibrations due to the hole localization. It can be facilitated by the qualitative difference in the lattice relaxation around the two centers that is clearly seen in Figs. 2 and 3. The completely relaxed configuration of the ions surrounding the Mn^{4+} electronic hole defect (see Fig. 2) corresponds to the positions of cores in region I that have appreciable displacements (more than or equal to 0.004 Å) from their perfect lattice sites. The cores of the six nearest neighbor oxygen ions are symmetrically displaced by about 0.1 Å towards the Mn^{4+} ion carrying the hole. The rest of the lattice relaxation comprises small displacements of the Mn and La ions (about 0.01 and 0.004 Å, respectively) out from the Mn^{4+} hole center.

By contrast, the ionic relaxation around the O^- hole center has the axial symmetry, with the largest lattice displacements of the nearby Mn ions (about 0.21 Å) along the axis away from the O^- hole center (see Fig. 3). These displacements cause the next two

Fig. 2. The core displacements (more than or equal to 0.004 Å) of the ions surrounding the Mn^{4+} electronic hole defect after the complete relaxation of cores and shells in the $LaMnO_3$ lattice

Fig. 3. The core displacements (more than or equal to 0.03 Å) of the ions surrounding the O^- electronic hole defect after the complete relaxation of cores and shells in the $LaMnO_3$ lattice

Table 3. Formation and polarization energies for localized holes in $LaMnO_3$: (a) for the pair potentials explored in this work; (c) for the pair potentials from Grimes [20] (Table 1) for Mn^{3+} and Mn^{4+} different valence states

	α-hole	$E^{\alpha}_{h,opt}$	$E^{\alpha}_{h,th}$	I^{α} ($E^{\alpha}_{\rm IV}$)	S^{α}_{opt}	S^{α}_{th}	U^{α}_{M}	R^{α}_{opt}	ΔR^{α}_{th}	E^{α}_{PES}
(a)	Mn^{4+}	2.56	1.73	47.41 (51.20)	−44.85	−45.68	−38.3	−6.55	−0.83	1.2
	O^{-}	4.86	2.48	−13.91	18.77	16.39	22.1	−3.33	−2.38	3.5
	La^{4+}	18.36	17.63	49.45 (49.45)	−31.09	−31.82	−27.4	−3.68	−0.73	17.0
(c)	Mn^{4+}	2.62	1.95	46.83 (51.20)	−44.27	−44.94	−38.1	−6.17	−0.67	1.2
	O^{-}	4.92	2.52	−13.82	18.74	16.34	22.0	−3.26	−2.40	3.5
	La^{4+}	18.42	17.84	49.45 (49.45)	−31.03	−31.61	−27.4	−3.63	−0.58	17.0

apical oxygen ions along the axis to move away from the O^{-} hole center by about 0.1 Å. The equatorial oxygen ions in the octahedron relax towards the hole center by about 0.03 Å. In-plane La ions also show appreciable displacements away from the O^{-} hole center. The qualitative difference in the symmetry of the lattice relaxation around the two centers implies the difference in the local vibrational modes, which can be used for experimentally probing the hole localization in $LaMnO_3$.

3.2. Photoemission spectra and in-crystal ionization potentials in $LaMnO_3$. Formation energies of the localized holes in the $LaMnO_3$ crystal

To evaluate the hole formation energy, we need to estimate the values of the unknown in-crystal ionization energies I^{α}. We suggest estimating the ionization potentials from the experimental photoemission spectroscopy (PES) data, which can be directly related to our calculations. In principle, PES at different excitation energies probes bonding states as well as nonbonding states. The latter, being ion-in-crystal-like, can be related to the Frank–Condon energies obtained in our calculations. In order to juxtapose experimental and calculated values, we must also take into account that the PES binding energy E_{PES} is measured with respect to the Fermi energy level E_F of the sample. Therefore, we write

$$I^{\alpha} + U^{\alpha}_{M} + R^{\alpha}_{opt} = E^{\alpha}_{PES} + E_F. \qquad (5)$$

In the PES spectra of $LaMnO_3$, there are two main photoemission bands around 3.5 and 6 eV binding energies at $T = 100$, 200 K for the HeI ($h\nu = 21.2$ eV) and HeII ($h\nu = 40.8$ eV) photon energies for which the O($2p$) photoionization cross-section is dominant [22]. The main maximum at 3.5 eV has been primarily assigned to the O($2p$) nonbonding states, whereas the second maximum is assigned to the Mn($3d$)–O($2p$) bonding states and the decrease of the O($2p$) character correlates with the decrease of the Mn($3d$)–O($2p$) hybridization strength. For higher energies with the HeII PES study, the $\sigma_{\rm Mn(3d)}/\sigma_{\rm O(2p)}$ cross-section ratio increases and a feature near 2.7 eV appears [22]. At high photon energies 500 eV and $T = 280$ K, the band at 3.5 eV is not clearly evident, but the band at 2.7 eV becomes dominant over the band at 6 eV, which stands for the maximum contribution of Mn($3d$) $3t_{2g}$ states at the binding energy of 2.7 eV [23]. The crystal field splitting between the Mn($3d$) $3t_{2g}$ and e_g states in $LaMnO_3$ has been estimated from the PES study to be about $\Delta_{CF} \approx 1.5$ eV [23]. The peak at 17 eV has been assigned to the La($5p$) states [23].

Thus, in accordance with the dominant contributions to the PES spectra of $LaMnO_3$ [22, 23], we assign the values $E^{\rm O}_{PES} \approx 3.5$ eV, $E^{\rm La}_{PES} \approx 17.0$ eV, and $E^{\rm Mn}_{PES} \approx 1.2$ eV, suggesting that the Mn hole formation process is associated with the electron photoionization from the e_g level. These maxima in the PES spectra correlate well with the maxima in the density of states for the O($2p$) and Mn($3d$) e_g valence bands in $LaMnO_3$ calculated within the local spin density approximation (LSDA) [21]. The corresponding schematic representation of the band structure in accordance with the assigned maxima of binding energies in the PES spectra [22, 23] in the scale of energies related to the crystal Fermi level E_F is shown in Fig. 4. The gap in the e_g electron band opened at E_F due to the lattice distortion (the JT effect and/or lattice mismatch effect) is shown in accordance with the PES crystal field splitting data [23]. The relevant electron excitations from the Mn($3d$) e_g, O($2p$), and La($5p$) valence band levels are schematically shown by arrows. The corresponding PES energies E^{α}_{PES} are summarized in Table 3.

Having assigned the E^{α}_{PES} energies, we now pro-

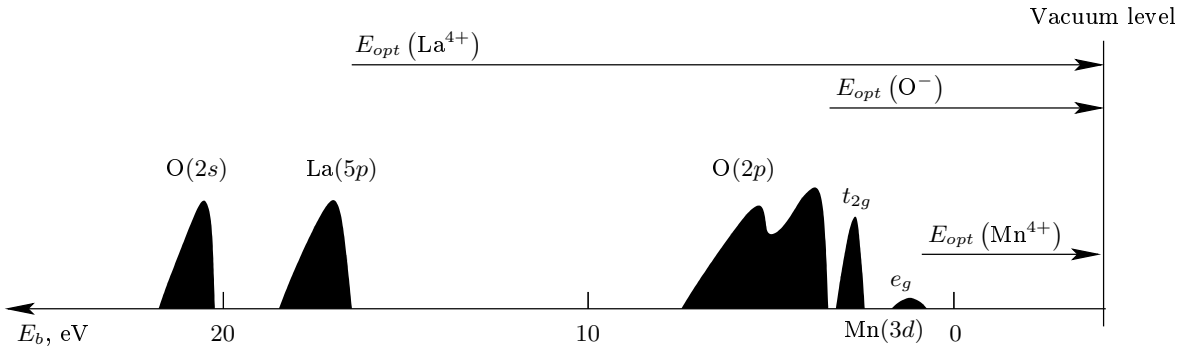

Fig. 4. A schematic representation of the valence band structure of the $LaMnO_3$ crystal, showing binding energies [22, 23] with respect to the crystal Fermi level E_F. The processes of the optical electron excitation from the Mn(3d) e_g, O(2p), and La(5p) valence bands to the vacuum level are shown by arrows. These optical excitation energies can be compared with experimental PES data [22, 23] and with the calculated values of optical energies E_{opt}, for the Mn^{4+}, O^-, and La^{4+} hole formation (Table 3)

ceed with the evaluation of the hole formation energies E_h^α. We first obtain the crystal Fermi energy using Eq. (5) and data for the La ion. We assume that the electronic density of the closed-shell La^{3+} ion is not significantly deformed by the crystalline field, and the in-crystal ionization energy I^{La} can therefore be plausibly estimated by the fourth standard ionization potential E_{IV} of a free La atom [24], presented in Table 3. This approximation is consistent with the full ionic charges adopted in our shell model parameterization. We note that the above approximation of a free cation is shown to be reliable only for closed-shell cations. This gives $E_F \approx 1.36$ eV for the Fermi energy of the $LaMnO_3$ crystal.

The situation is more complicated for manganese and oxygen. The Mn^{3+} ion has a nonclosed 3d shell with four electrons in it, and we therefore expect the in-crystal ionization energy I^{Mn} to be different from the fourth ionization potential of a free Mn atom. Because the O^{2-} ion is only stabilized by the crystalline field, it has a negative ionization potential that cannot be defined in a nonspeculative way. Using the Mn(3d) and O(2p) related maxima in the PES spectra, E_{PES}^α, and the obtained value $E_F \approx 1.36$ eV, we can now estimate the effective ionization energies I^α for manganese and oxygen in the $LaMnO_3$ crystal from Eq. (5). These values are presented in Table 3, with the free metal ionization potentials [24] given in brackets for comparison. The O^{2-} in-crystal ionization potential I^{O} (negative electron affinity of O^-) is then estimated to be -13.91 eV. The absolute value of this potential is within the limits of O^- electron affinities calculated for many oxide compounds in Ref. [25] using the embedded cluster *ab-initio* method. Those calculations predicted 10.6 eV for MgO and 12.9 eV for ThO_2. Taking the semiempirical nature of our calculations into account, we find this agreement quite good.

The optical and thermal energies of the hole formation, $E_{h,opt}^\alpha$ and $E_{h,th}^\alpha$, are calculated using these effective values of the in-crystal ionization energies in accordance with Eq. (4) and presented in Table 3. Taking the crystal field splitting effect into account, we have found that the electronic hole is marginally more stable at the Mn site than at the O site in the $LaMnO_3$ lattice, but the energy difference between the thermal energies of the hole formation, $E_{h,th}^\alpha$, is too small (0.75 eV). This result rather suggests that both possibilities should be treated seriously. That is, providing the balance between the localization and relaxation energies favors the possibilities for the hole self-trapping at the Mn and O sites, the electronic hole in $LaMnO_3$ is likely to be localized on the manganese, or on both the oxygen anion and the transition metal cation, rather than on the oxygen ion alone.

To assess the accuracy of the calculated energies of the hole formation and lattice relaxation, we need to discuss the following issue related to the pair potentials used in these calculations. The energies presented in Table 3(a) were obtained using the pair potentials listed in Table 1(a). To verify the robustness of our results, we repeated the same calculations using the potentials in [20], which give close values for the dielectric constants in $LaMnO_3$ (see Table 2(c)), but were specially optimized to treat different Mn^{3+} and Mn^{4+} charge states. The calculated values of formation and polarization energies for the localized holes Mn^{4+}, O^-, and La^{4+} and the energies deduced in Eq. (4) using these pair potentials are presented in Table 3(c). These

calculations demonstrate that the hole relaxation energy of Mn^{4+} is decreased by 0.16 eV if we account for the change in the short-range potentials caused by the change of the Mn charge state. Comparing with our results, we can see good coincidence for the similar values and for the thermal and optical energies of hole formation.

4. OPTICAL CHARGE TRANSFER TRANSITIONS IN $LaMnO_3$

Polaronic-type electron charge carriers mostly determine specific transport properties of CMR materials in their high-temperature insulating paramagnetic phase, which are always associated with photo-induced charge transfer transitions. In hole-doped systems of perovskite manganites $R_{1-x}A_xMnO_3$, the most important charge transfer transitions associated with localized charge carriers are apparently those involving Mn^{4+} and O^- self-trapped holes. In this section, using the derived values of the in-crystal ionization energies, we calculate energies of the main charge transfer transitions suggesting that holes could be localized at the Mn or O sites. We analyze the contribution of these charge transfer transitions to the experimental optical conductivity in nonstoichiometric or slightly hole-doped $LaMnO_3$ crystals to make the assignment of the bands in the optical conductivity spectrum more clear-cut and to verify our shell model approach. We now proceed with a brief analysis of the optical conductivity spectra.

4.1. Analysis of the optical conductivity spectra in $LaMnO_3$

The room-temperature optical conductivity spectrum of $LaMnO_3$ measured in [15] is shown by solid curve *1* in Fig. 5*a* in the spectral region 0 to 8 eV (reproduced from the original data with a permission of Arima and Tokura [15, 16]). This spectrum is very similar to that measured by Okimoto et al. at $T = 9$ K [26]. It reveals the optical gap near 1.3 eV and includes several broad absorption bands with maxima near 2.3, 5, and 9 eV. The gap is assumed to be of the charge transfer type [15]. The first transition around 2.3 eV has been suggested to be of the O($2p$)–Mn($3d$) character. The band near 5 eV is thought to be due to the excitations to a higher lying Mn $3d$ e_g antiparallel spin configuration, separated by a Hund's rule coupling energy. The wide band observed around 9 eV in the optical conductivity spectrum is assigned to the O($2p$)–La($5d$) interband optical transition [15].

The optical spectra measured in hole-doped manganese oxides show striking changes over a wide photon region (0 to 6 eV) as the temperature and doping concentration change. In the $La_{1-x}Sr_xMnO_3$ system, with increasing doping concentration ($x = 0$ to 0.3, $T = 9$ K [26]), the excitations around 2.3 and 5 eV shift appreciably to lower energies. However, the principal changes occur in the low-energy mid-infrared spectral region stemming from the filling of the gap because of the hole doping. In the insulating paramagnetic phase of hole-doped manganites, there are two features clearly observed in the experimental mid-infrared optical conductivity, around 0.6 eV [18, 26] and around 1.2–1.5 eV [27, 28]. The optical band around 0.6 eV seems to be associated with polaronic-type charge carriers in doped CMR manganites, and the consistent value of the activation energy of about 0.15 eV was measured for the hopping conductivity in the adiabatic temperature limit [29, 30]. The origin of these features is still a subject of many controversial discussions. It is well known that the $LaMnO_3$ crystal has a strongly distorted orthorhombic structure at low temperatures, which in many works is ascribed due to a strong electron–phonon interaction stemming from the JT effect inherent for Mn^{3+} ion in the octahedral oxygen configuration. In this case, the e_g bands split into two subbands separated by the JT energy E_{JT}. Because the on-site d–d transitions are dipole-forbidden, these mid-infrared peaks around 0.6 and 1.2–1.5 eV were qualitatively explained as occurring because of an electron transition from an occupied site Mn^{3+} to an unoccupied site Mn^{4+} and an adjacent occupied site Mn^{3+}, respectively [1].

In a recent theoretical study of the optical conductivity spectra of $3d$ transition metal perovskites $LaMO_3$ (M = Ti–Cu) [31] using the local spin density approximation method (LSDA + U), the authors estimated the role of lattice distortions in the band structure calculations and concluded that the JT structural distortions play a crucial role in opening the optical gap in the $LaMnO_3$ Mn($3d$) e_g valence band. Considering the experimentally observed distorted structure of the $LaMnO_3$ crystal, the direct gap in the LSDA study has been estimated as appoximately 0.7 eV, which is less than the observed optical gap (about 1.3 eV [15, 26]). There are also some discrepancies observed at higher energies between the experimental optical conductivity in $3d$ transition metal perovskites $LaMO_3$ and the calculated optical conductivity considering contributions from the interband and intraband transitions for the perfect lattice [31], which complicates the assignment of the optical bands. In addition, the contribution from

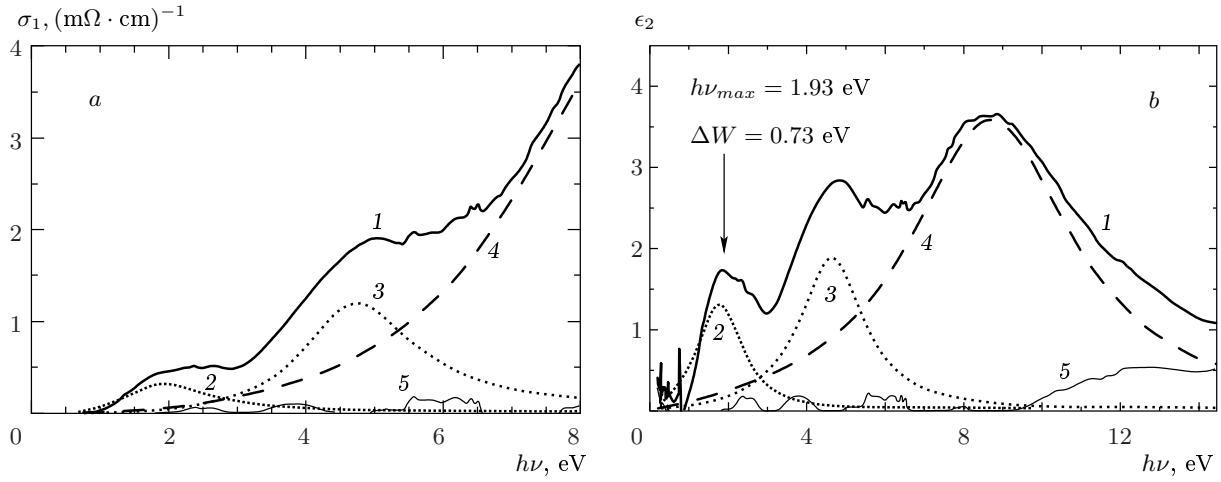

Fig. 5. *a*) The experimental optical conductivity spectrum of the $LaMnO_3$ crystal [15] (curve *1*, $T = 300$ K) represented by the contributions from the three Lorentz oscillators in accordance with the dispersion analysis of the imaginary part of the dielectric function ϵ_2 shown in Fig. 5*b*. *b*) The experimental ϵ_2 spectrum of $LaMnO_3$ (curve *1*, $T = 300$ K) represented by a sum of three main Lorentzian shaped bands: 1.93, 4.75, and 9.07 eV (drawn by curves *2*, *3*, and *4*, respectively). The rest of the ϵ_2 spectrum after subtraction of the Lorentzian bands is shown by line *5*. The Lorentzian band parameters are given in Table 4 together with the estimated oscillator strengths f_i

the charge transfer transitions to the optical conductivity in the nonstoichiometric lattice must be taken into account to describe the optical conductivity at low energies satisfactorily and to clarify the assignment of the optical bands in the $LaMnO_3$ crystal.

To estimate the contribution of the charge transfer transitions to the experimental optical conductivity of the $LaMnO_3$ crystal, shown by curve *1* in Fig. 5*a*, we have analyzed the imaginary part $\epsilon_2(\nu)$ of the dielectric function [15, 16]. For this purpose, we represented the $\epsilon_2(\nu)$ spectrum, shown by curve *1* in Fig. 5*b*, as the sum of the first three main bands with Lorentzian lineshapes,

$$\epsilon_2(\nu) = \sum_i \frac{\nu_{pi}^2 \gamma_i \nu}{(E_i^2 - \nu^2)^2 + \gamma_i^2 \nu^2}, \qquad (6)$$

where $(\nu_{pi}/E_i)^2 = f_i$ is the oscillator strength, ν_{pi} is the plasma frequency, γ_i is the bandwidth, and E_i is the resonance frequency of the ith oscillator. The three Lorentzian bands with the maxima E_i at 1.93, 4.75, and 9.07 eV and the respective widths γ_i of 1.46, 2.0, and 5.1 eV are represented by curves *2*, *3*, and *4* in Fig. 5*b*. The rest of the imaginary part of the dielectric function after subtraction of the Lorentzian bands is shown by curve *5*. The Lorentzian band parameters together with the estimated oscillator strengths are given in Table 4. These Lorentzian bands contribute to the experimental optical conductivity spectrum, as shown by the corresponding lines in Fig. 5*a*, with more details at low energies.

Table 4. Parameters of the imaginary part ϵ_2 of the dielectric function [15, 16] represented by the sum of Lorentzian shaped bands

E_i, eV	γ_i, eV	ν_{pi}^2, eV^2	f_i
1.93	1.46	1.895	0.51
4.75	2.0	4.22	0.187
9.07	5.1	12.75	0.155

4.2. Calculation of charge transfer transition energies

Using the Born–Haber cycle and the shell model, we can consider both thermally assisted and optical charge transfer processes. This can be illustrated for a hypothetical transformation of two ions $X^{(m+1)+}$ and $Y^{(n-1)+}$ into X^{m+} and Y^{n+} with an electron transferred from Y to X (or a hole from X to Y),

$$X^{(m+1)+} + Y^{(n-1)+} \to X^{m+} + Y^{n+}. \qquad (7)$$

There are two basic steps: 1) removing an electron from the in-crystal $Y^{(n-1)+}$ ion to infinity, outside the crystal; 2) adding an electron from the infinity, outside the crystal, to the in-crystal $X^{(m+1)+}$ ion. The steps are

standard within the shell model. Whether shells alone or shells and cores are relaxed depends on which transition is being calculated. In the case of a thermally assisted hopping, the shell and core positions are considered to be fully relaxed in both charge states and the transition energy is denoted by E_{th}. Comparison of the two charge states gives an additional indication which species are more stable. For optical transitions, the Franck–Condon approximation is used and the transition energies E_{opt} are calculated on the assumption that only shells can relax (corresponding to the full electronic polarization), whereas the cores remain in the positions corresponding to the initial state. The major contributions into these energies come from ionization energies $I_n^{\rm Y}$, $I_{(m+1)}^{\rm X}$; the Madelung and polarization terms, whose cumulative energies for the defect configuration corresponding to the charge transfer transition considered, $S[{\rm X}^{m+}, {\rm Y}^{n+}]_{opt,th}$, result from the Mott–Littleton calculations (as in Eq. (4)). If the charge transfer includes a localized hole in thermal equilibrium in the initial state (the related values in the $LaMnO_3$ lattice are presented as S_{th}^{α} in Table 3), the corresponding thermal energy $S[{\rm X}^{(m+1)+}, {\rm Y}^{(n-1)+}]_{th}$ of the initial defect configuration must be subtracted. Thus, the thermal and optical energies of the charge transfer transitions can be calculated using the formulas

$$E_{opt} = I_n^{\rm Y} - I_{m+1}^{\rm X} + S[{\rm X}^{m+}, {\rm Y}^{n+}]_{opt} - \\ - S[{\rm X}^{(m+1)+}, {\rm Y}^{(n-1)+}]_{th}, \quad (8)$$

$$E_{th} = I_n^{\rm Y} - I_{m+1}^{\rm X} + S[{\rm X}^{m+}, {\rm Y}^{n+}]_{th} - \\ - S[{\rm X}^{(m+1)+}, {\rm Y}^{(n-1)+}]_{th}. \quad (9)$$

Evidently, there is some dependence on the separation of X and Y. The charge transfer optical transitions for nearest neighbors are likely to dominate and the relevant key cases have been calculated. If X and Y are the same (symmetric), the ionization terms cancel each other, as for the intervalence charge transfer transition

$$Mn^{4+} + Mn^{3+} \rightarrow Mn^{3+} + Mn^{4+}.$$

We here emphasize that the calculations of charge transfer transitions between the metal Mn sublattice ions are more reliable because they do not depend on the difference between the Madelung potentials of the two sublattices, nor on the phenomenologically deduced parameter of the O^{2-} in-crystal ionization potential.

The cumulative thermal S_{th} and optical S_{opt} energies following from the Mott–Littleton calculations for the charge transfer transitions involving Mn^{4+} and O^- species, and those characterizing fundamental electronic transitions in the $LaMnO_3$ lattice (e.g., the Mn($3d$) gap transition, O($2p$)–Mn($3d$), and O($2p$)–La($5d$)) are presented in Table 5 by transitions 1–3 and 4–6, respectively. To calculate the optical and thermal energies of the charge transfer transitions, we used a self-consistent set of the ionization potentials (see Table 3(a)) derived by matching the calculated optical energies of the hole formation with the photoemission experimental energies and the standard ionization potentials for a free La atom. We must also estimate the third in-crystal ionization potential of Mn, $I_{\rm III}^{\rm Mn}$. We suggest that it should be shifted in-crystal from the standard value for a free Mn atom (33.67 eV [24]) by the same value as the fourth potential of Mn (from the standard value 51.2 eV), by subtracting the crystal field splitting effect ($\Delta_{CF} \approx 1.5$ eV); we thus calculate in-crystal

$$I_{\rm III}^{\rm Mn} = 33.67 - (51.2 - (47.41 + \Delta_{CF}/2)) = 30.63 \text{ eV}.$$

Taking the standard value $I_{\rm III}^{\rm La} = 19.18$ eV, the calculated optical energy of the fundamental transition of the charge transfer character O($2p$)–La($5d$),

$$E_{opt} = I^{\rm O} - I_{\rm III}^{\rm La} + S[{\rm La}^{3+}, {\rm O}^{2-}]_{opt} = 8.93 \text{ eV}$$

(see Table 5, transition No. 6) correlates well with the maximum of the broad band in the ϵ_2 function near 9.07 eV (curve *4* in Fig. 5*b*). This encouraging consistency between the experimental and calculated energies allows us to suggest that the earlier estimated in-crystal value $I^{\rm O} = -13.91$ eV provides a reasonable value in this shell model calculation. We also calculated the optical energy of the fundamental transition of the charge transfer character O($2p$)–Mn($3d$),

$$E_{opt} = I^{\rm O} - I_{\rm III}^{\rm Mn} + S[{\rm Mn}^{3+}, {\rm O}^{2-}]_{opt} = 5.61 \text{ eV}$$

(see Table 5, transition No. 5). We suggest that the relevant transition should correlate with the broad optical band observed in the ϵ_2 function near 4.75 eV (curve *3* in Fig. 5*b*). Our calculations therefore predict transitions which appear to correlate with the maxima of the major broad-band features in the optical conductivity spectrum. The calculated optical energy for the transition between the Mn($3d$) valence band and the upper Hubbard Mn($3d$) band is estimated to be

$$E_{opt} = I_{\rm IV}^{\rm Mn} - I_{\rm III}^{\rm Mn} + S[{\rm Mn}^{3+}, {\rm Mn}^{3+}]_{opt} = 3.72 \text{ eV}$$

(see Table 5, transition No. 4), predicting a band gap of the Mott–Hubbard type in the $LaMnO_3$ crystal. This

Table 5. Calculated optical (E_{opt}) and thermal (E_{th}) energies for the main charge transfer transitions in $LaMnO_3$; S_{opt} and S_{th} are resultant calculated values of the sum of defect energies for the corresponding charge transfer process

No.	Charge transfer transition	E_{opt}, eV	Exp., eV	E_{th}, eV	S_{opt}, eV	S_{th}, eV
1	$Mn^{4+} + Mn^{3+} \to Mn^{3+} + Mn^{4+}$	1.33	–	0.00	−44.35	−45.68
2	$O^- + Mn^{3+} \to O^{2-} + Mn^{4+}$	1.43 (2.29)	1.93	−0.75 (0.12)	−43.50	−45.66
3	$Mn^{4+} + O^{2-} \to Mn^{3+} + O^-$	2.98 (2.12)	1.93	0.75 (−0.12)	18.62	16.39
4	$2Mn^{3+} \to Mn^{4+} + Mn^{2+}$	3.72	3.5 [27], 3.2 [32]	2.68	−13.06	−14.10
5	$Mn^{3+} + O^{2-} \to Mn^{2+} + O^-$	5.61 (4.75)	4.75	3.50	50.15	48.04
6	$La^{3+} + O^{2-} \to La^{2+} + O^-$	8.93	9.07	6.47	42.02	39.56

Transitions Nos. 4, 5, and 6 are associated with the Mn($3d$) gap, O($2p$)–Mn($3d$), and O($2p$)–La($5d$) transitions, respectively.

value agrees well with the assigned transition experimentally observed near 3.5 eV in $Nd_{0.7}Sr_{0.3}MnO_3$ [27] and near 3.2 eV in $La_{0.825}Sr_{0.175}MnO_3$ [32]. A small contribution to the experimental optical conductivity can be observed around 3.7 eV in the $LaMnO_3$ crystal, as shown by curve *5* in Fig. 5*b* resulting from our dispersion analysis.

Having assigned the fundamental electronic transitions in the $LaMnO_3$ crystal in accordance with the results of our calculations, which are also consistent with the consideration in Ref. [27], we note that the assignment of the optical conductivity band around 2.3 eV still remains controversial. In the earlier study [15], this band was associated with the fundamental charge transfer transition of the O($2p$)–Mn($3d$) e_g character, whereas the band at about 5 eV was associated by the authors with the excitations to a higher lying Mn $3d$ e_g antiparallel spin configuration, separated by the Hund's rule coupling energy. However, our results allow us to argue that an alternative interpretation of this transition obtained in this work can be correct. We suggest that the band at about 2.3 eV is rather associated with the presence of Mn^{4+} and/or O^- localized holes in the $LaMnO_3$ crystal, which is known to exhibit a strongly nonstoichiometric behavior with respect to the oxygen content, up to 0.1 in as-grown crystal.

Indeed, if an optical band is associated with a charge transfer transition in a crystal lattice, its maximum position $h\nu_{max}$ and the half-width ΔW are known to be related by a simple formula in the high-temperature limit [33],

$$h\nu_{max} = \frac{\Delta W^2}{16kT\ln 2}. \qquad (10)$$

We can invoke this expression to verify the charge transfer transition character of the bands associated with the photo-induced hopping conductivity of the localized charge carriers. Using this expression, the estimates for $T = 300$ K show a very encouraging consistency between the half-width and the maximum energy of the first Lorentzian band (curve *2* in Fig. 5*b*, with the parameters given in Table 4): from $\Delta W \approx 0.73$ eV, we obtain $h\nu_{max} \approx 1.92$ eV, which matches well the maximum position estimated to be near 1.93 eV from the dispersion analysis of the ϵ_2 function. This is consistent with the view that this transitions could be of the charge transfer type, associated with the presence of localized electronic charge carriers in the $LaMnO_3$ crystal lattice.

The main contributions to the optical conductivity are then expected from the following charge transfer transitions:

1) the intervalence Mn^{3+}/Mn^{4+} charge transfer transition,

$$Mn^{4+} + Mn^{3+} \to Mn^{3+} + Mn^{4+},$$

$$E_{opt} = S[Mn^{3+}, Mn^{4+}]_{opt} - S_{th}^{Mn} = 1.33 \text{ eV},$$

2) the transition of the O^- self-trapped hole to a neighboring manganese ion,

$$O^- + Mn^{3+} \to O^{2-} + Mn^{4+},$$

$$E_{opt} = I_{IV}^{Mn} - I^O + S[O^-, Mn^{3+}]_{opt} - S_{th}^O = 1.43 \text{ eV},$$

3) the transition of the Mn^{4+} self-trapped hole to a neighboring oxygen ion,

$$Mn^{4+} + O^{2-} \to Mn^{3+} + O^-,$$

$$E_{opt} = I^O - I_{IV}^{Mn} + S[O^{2-}, Mn^{4+}]_{opt} - S_{th}^{Mn} = 2.98 \text{ eV}$$

(see transitions Nos. 1–3, respectively, in Table 5).

Analyzing all calculated and experimental optical energies given in Table 5, we can conclude that the agreement is much better for the calculations not involving the in-crystal ionization potentials of manganese, $I_{\rm III}^{\rm Mn}$ and $I_{\rm IV}^{\rm Mn}$, or in the case where their difference enters and the inaccuracy due to these terms cancels out. Relying on the correlation between the calculated and experimental optical energies, we can try to refine the values of $I_{\rm III}^{\rm Mn}$ and $I_{\rm IV}^{\rm Mn}$, whose in-crystal determination presents difficulties due to a nonclosed $3d$ shell of the Mn^{3+} ion. Indeed, expecting the calculated optical energy of the fundamental transition of the charge transfer character O($2p$)–Mn($3d$),

$$E_{opt} = I^{\rm O} - I_{\rm III}^{\rm Mn} + S[{\rm Mn}^{3+}, {\rm O}^{2-}]_{opt} = \\ = -13.91 - 30.63 + 50.15 = 5.61 \text{ eV}$$

(see Table 5, transition No. 5) to be correlated with the broad optical band observed in the ϵ_2 function near 4.75 eV (curve *3* in Fig. 5*b*), we can refine the third in-crystal ionization potential of manganese as $(I_{\rm III}^{\rm Mn})^* = 31.49$ eV and, correspondingly, $(I_{\rm IV}^{\rm Mn})^* = 48.27$ eV. Using these corrected values, we recalculated the energies of transitions Nos. 2 and 3 in Table 5 associated with the charge transfer transitions of O^- and Mn^{4+} self-trapped holes and obtained close values of optical energies, $E_{opt} = 2.29$ eV and $E_{opt} = 2.12$ eV, respectively. These corrected values for the optical charge transfer transition energies are presented in brackets in Table 5 for transitions Nos. 2 and 3. We suggest that these transitions, $Mn^{4+} + O^{2-} \to Mn^{3+} + O^-$ and $O^- + Mn^{3+} \to O^{2-} + Mn^{4+}$, associated with the hole transfer along the chain Mn^{4+}–O^{2-}–Mn^{3+} could be responsible for the band around 2.3 eV in the optical conductivity spectrum (the related band in the ϵ_2 spectrum has the maximum energy 1.93 eV) of the as-grown nonstoichiometric $LaMnO_3$ crystal. If the band is thus assigned, the net oscillator strength of this band, $f_i = 0.51$ (see Table 4) must depend on the concentration of the localized holes as $f_i = f_{CT}/x$, thereby providing an estimate of the oscillator strength for the charge transfer transition, f_{CT}. The typical value $x \approx 0.1$ for an as-grown $LaMnO_3$ crystal gives an estimate for the oscillator strength consistent with the transition of the charge transfer type.

The negative value of the thermal energy, $E_{th} = -0.75$ eV, for transition No. 2 in Table 5 indicates a more thermally stable state of the Mn^{4+} hole compared to the O^- hole state, in accordance with our results for the thermal energies E_{th}^{α} of the holes formation (Table 3(a)) based on preliminary estimates for the fourth in-crystal ionization potential of the manganese ion. Using the refined value $I_{\rm IV}^{\rm Mn} = 48.27$ eV deduced from the comparison between the calculated and experimental optical energies, we now derive the respective thermal energies 0.12 and -0.12 eV for transitions Nos. 2 and 3. This result reinforces our arguments made above that the electronic hole can be thermally stable on both the transition metal cation and the oxygen anion in the $LaMnO_3$ crystal.

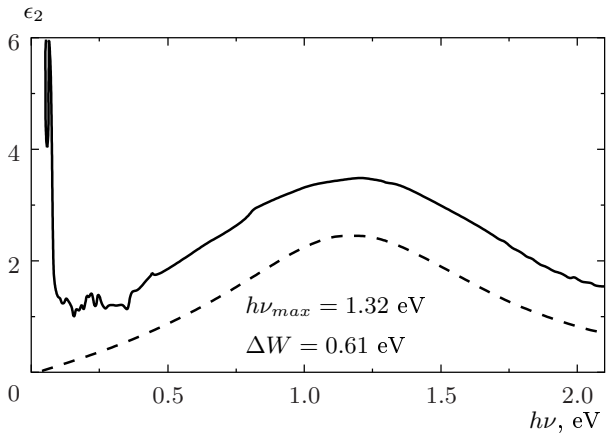

Fig. 6. The experimental (solid line) ϵ_2 spectrum of $La_{7/8}Sr_{1/8}MnO_3$ [28] ($T = 300$ K) approximated by the Lorentzian shaped band (dashed line)

In accordance with our shell model calculations, the intervalence charge transfer transition $Mn^{4+} + Mn^{3+} \to Mn^{3+} + Mn^{4+}$ is predicted to have the optical energy $E_{opt} = 1.33$ eV (Table 5, transition No. 1); compared with the energy of the optical gap in $LaMnO_3$, it is not observable in an as-grown pure crystal.

Because of the doping effect, the optical spectra in CMR manganese oxides show striking changes over a wide photon region (0 to 6 eV). In the $La_{1-x}Sr_xMnO_3$ system, with increasing the doping concentration from $x = 0$ to 0.3 at $T = 9$ K [26], the optical conductivity bands around 2.3 and 5 eV shift to lower energies by more than 0.5 eV. We have analyzed the low-energy ϵ_2 function in a slightly doped $La_{7/8}Sr_{1/8}MnO_3$ compound [28], and found it to be well described by the Lorentzian curve with the maximum at 1.32 eV and the half-width of 0.61 eV, as presented in Fig. 6. We emphasize that the maximum position of this band and its half-width are also in a good correlation with the formula describing a transition of the charge transfer character (see Eq. (10)): from $\Delta W \approx 0.61$ eV, we obtain $h\nu_{max} \approx 1.34$ eV, which matches well the maximum position observed experimentally. It is reasonable to suggest that this band is of the same origin as the band at

$\epsilon_2 = 1.93$ eV in the pure $LaMnO_3$ compound, assigned to transitions Nos. 2 and 3 in Table 5 and shifted by about 0.5 eV to lower energies because of the hole interaction effect in CMR systems. Using this line of reasoning, we can also suggest that the 0.6 eV band [18, 26] in the optical conductivity of CMR compounds is due to the intervalence charge transfer transition $Mn^{4+} + Mn^{3+} \rightarrow Mn^{3+} + Mn^{4+}$ and is associated with the photo-induced hopping conductivity of Mn^{4+} localized holes, with the consistent value of hopping conductivity activation energy of approximately 0.15 eV measured in the adiabatic temperature limit [29, 30].

The results given are based on the shell model parameters (Table 1(a)), which were fitted to give good values for both the dielectric constants and the TO modes. When we use the second set of the shell model parameters, determined primarily using the oxide structures MnO, $LaMnO_3$, and Ca_2MnO_4 [20] (Table 1(c)), the resulting energies are very similar for the low-energy optical charge transfer transition band near 2.3 eV, but the predicted energies are about 1.5 eV higher for 5 eV optical band.

5. CONCLUSIONS

In this paper, we explore the role of electronic and ionic polarization energies in the physics of CMR materials. In particular, we examine energies associated with the localized Mn^{4+} and O^- holes in the lattice of the «parent» $LaMnO_3$ compound. Our calculations are done for the idealized cubic perovskite $LaMnO_3$ structure, which is relevant to the nonmagnetic quasicubic perovskite structure experimentally observed at high temperatures $T \geq 400$ K $> T_N \approx 140$ K. To estimate the polarization energy terms, we use a fully ionic shell model. The shell model parameters that we derive satisfy the equilibrium conditions for the quasicubic perovskite structure $LaMnO_3$ and agree well with experimental values of the static and high-frequency dielectric constants as well as the TO phonons.

As a result of our shell model calculations, we find that on one hand, there is a huge difference between the hole relaxation energies on the oxygen and manganese sites, which indicates a strong electron–phonon interaction in the case of a hole localized at the O site. On the other hand, the difference that we find between the thermal energies of the Mn^{4+} and O^- holes is too small. This means that we must seriously consider the possibility that the electronic hole in $LaMnO_3$ is localized on the manganese, or on both the oxygen anion and the transition metal cation, rather than on the oxygen ion alone. If so, this system would be similar to many other transition metal oxides.

Assuming that holes in the $LaMnO_3$ crystal can localize in either or in both the Mn and O sublattices, we estimate the main associated optical charge transfer transition energies, which we relate to the experimentally observed optical conductivity spectra. Applying the Mott–Littleton approach, we estimate the charge transfer transition energies within the Born–Hyber cycle using the in-crystal ionization potentials for ions in the $LaMnO_3$ crystal obtained in our study of the experimental photoemission spectra.

Our analysis allows us to suggest a new interpretation of the main bands in the optical conductivity spectrum near 2.3 and 5 eV. We suggest that the band around 5 eV is associated with the fundamental $O(2p)$–$Mn(3d)$ transition of the charge transfer character, whereas the band near 2.3 eV is rather associated with the presence of Mn^{4+} and/or O^- self-trapped holes in the nonstoichiometric $LaMnO_3$ compound.

To summarize, we believe that the results of this work demonstrate the applicability and usefulness of the shell model approach to preliminary modeling of polaron-related features in complex oxides such as CMR materials, and hope that they will stimulate further theoretical and experimental studies of the character and properties of hole states in these materials.

The authors thank J. Gale for making available General Utility Lattice Program (GULP) used in the present calculations. We greatly appreciate Y. Tokura and T. Arima for providing us with the original reflectivity spectra in $LaMnO_3$. We thank F. Mayr and coauthors for the permission to reproduce their experimental data. We would also like to thank W. C. Mackrodt and A. Ionov for the useful information. We are grateful to R. W. Grimes and D. J. Bradfield for fruitful discussions and for making available to us one set of interatomic potentials. We are also grateful for the Royal Society/NATO support of the visit to the University College London of one of us (N. N. K.).

REFERENCES

1. A. J. Millis, R. Mueller, and B. I. Shraiman, Phys. Rev. B **54**, 5405 (1996).

2. H. L. Ju, H. C. Sohn, and Kannan M. Krishnan, Phys. Rev. Lett. **79**, 3230 (1997).

3. G. D. Watkins, Inst. Phys. Conf. Ser. **31**, 95 (1977); K. M. Lee, Le Si Dang, and G. D. Watkins, Sol. St.

Comm. **35**, 527 (1980); D. Jeon, H. P. Gislason, and G. D. Watkins, Mater. Sci. Forum **10–12**, 851 (1986).

4. J. H. Harding and A. M. Stoneham, J. Phys. C **15**, 4649 (1982).

5. B. G. Dick and A. W. Overhauser, Phys. Rev. **112**, 90 (1958).

6. W. Cochran, Crit. Rev. Sol. St. Sci. **2**, 1 (1971).

7. A. M. Stoneham, M. J. L. Sangster, and P. W. Tasker, Phil. Mag. B **44**, 603 (1981).

8. D. G. Muxworthy and C. R. A. Catlow, Phil. Mag. B **37**, 63 (1978).

9. R. Englman, *The Jahn–Teller Effect in Molecules and Crystals*, Wiley-Interscience, London–New York (1972).

10. A. L. Shluger and A. M. Stoneham, J. Phys.: Condens. Matter **5**, 3049 (1993).

11. N. F. Mott and M. J. Littleton, Trans. Faraday Soc. **34**, 485 (1938); C. R. A. Catlow and W. C. Mackrodt, *Computer Simulations of Solids*, Springer-Verlag, Berlin (1982); C. R. A. Catlow and A. M. Stoneham, J. Chem. Soc. Faraday Trans. II **85**, 505 (1989).

12. J. D. Gale, Phil. Mag. B **73**, 3 (1996); J. Chem. Soc. Faraday Trans. **93**, 629 (1997).

13. C. R. A. Catlow and A. M. Stoneham, J. Phys. C **16**, 4321 (1983).

14. C. R. A. Catlow, W. C. Mackrodt, M. J. Norgett, and A. M. Stoneham, Phil. Mag. **35**, 177 (1977).

15. T. Arima and Y. Tokura, J. Phys. Soc. Jap. **64**, 2488 (1995).

16. T. Arima and Y. Tokura, Private communication.

17. M. S. Islam, M. Cherry, and C. R. A. Catlow, J. Sol. St. Chem. **124**, 230 (1996).

18. A. V. Boris, N. N. Kovaleva, A. V. Bazhenov et al., Phys. Rev. B **59**, R697 (1999).

19. A. V. Boris, N. N. Kovaleva, A. V. Bazhenov et al., J. Appl. Phys. **81**, 5756 (1997).

20. R. Grimes and D. Bradfield, Private communication.

21. W. E. Pickett and D. J. Singh, Phys. Rev. B **53**, 1146 (1996).

22. T. Saitoh, Phys. Rev. B **56**, 8836 (1997).

23. J. H. Park, C. T. Chen, S.-W. Cheong et al., Phys. Rev. Lett. **76**, 4215 (1996).

24. D. R. Lide, *Handbook of Chemistry and Physics*, CRC Press, London (1993).

25. J. H. Harding and N. C. Pyper, Phil. Mag. Lett. **71**, 113 (1995).

26. Y. Okimoto, T. Katsufuji, T. Ishikawa et al., Phys. Rev. B **55**, 4206 (1997).

27. H. J. Lee, J. H. Jung, Y. S. Lee et al., Phys. Rev. B **60**, 5251 (1999).

28. F. Mayr, C. Hartinger, M. Paraskevopoulos et al., Phys. Rev. B **62**, 15673 (2000).

29. M. Jaime, M. B. Salamon, M. Rubinstein et al., Phys. Rev. B **54**, 11914 (1996).

30. A. Machida, Y. Morimoto, and A. Nakamura, Phys. Rev. B **58**, 12540, R4281 (1998).

31. I. Solovyev, N. Hamada and K. Terakura, Phys. Rev. B **53**, 7158 (1996).

32. K. Takenaka, Y. Sawaki, R. Shiozaki, and S. Sugai, Phys. Rev. B **62**, 13864 (2000).

33. N. S. Hush, Prog. Inorg. Chem. **8**, 391 (1967).